EUROPEAN JOURNAL OF BIOMEDICAL AND PHARMACEUTICAL SCIENCES
http://www.ejbps.com

ISSN 2349-8870
Volume: 5
Issue: 5
485-489
Year: 2018

HEMORRHAGE LESIONS SEGMENTATION AND DETECTION

Sudipta Roy[1] and Prof. Samir Kumar Bandyopadhyay*[2]

[1]Department of Computer Science and Engineering, Institute of Computer Technology (UVPCE), Ganpat University, Ahmadabad 380060, India.
[2]Advisor to Chancellor, JIS University, India.

***Corresponding Author: Prof. Samir Kumar Bandyopadhyay**
Advisor to Chancellor, JIS University, India.

Article Received on 21/02/2018 **Article Revised on 15/03/2018** **Article Accepted on 04/04/2018**

ABSTRACT
Accurate identification of brain abnormalities as hemorrhage lesions is the critical task in planning appropriate therapy. CAD systems have been the focus of several research activities, and it is solely based on the idea of analyzing images of different types of brain abnormalities by implementing improved image processing algorithms. In this paper, an approach is used to detect the hemorrhage abnormalities from MRI scan images of the brain.

KEYWORDS: Hemorrhage, Segmentation, Lesions.

INTRODUCTION

In modern times, automated diagnosis involves image segmentation step which is used to extract the abnormal lesions from brain MRI. The different abnormalities types differ in many computerized aspects such as nature, size, its shape, volume, number and its locations of lesions. The term abnormalities used to generalize the tumor, hemorrhage, and stroke because using automated system classification of different types of abnormalities is very difficult. Brain image segmentation attempts to label pixels by tissue type. Appropriate segmentation methods have a high correlation with image acquisition modality, the tissue of interest. Since MRI provides a superior contrast of soft tissue structures, it is the choice of method for imaging the brain. The detection of abnormalities is essential in the diagnosis and management of a variety of intracranial diseases including hypertensive hemorrhage, hemorrhagic infarction, brain tumor, cerebral aneurysm, vascular malformation, trauma, hemorrhagic changes following radio- or chemotherapy, and hemorrhagic pial metastasis. CAD systems incorporate computers to add a new dimension to physicians for achieving a faster and more accurate diagnosis. Development of such CAD system is challenging since they combine the elements of artificial intelligence and digital images processing. This work proposes a CAD system to assist the radiologist for the detection of hemorrhages in MRI scan images of the human brain to identify their natures.

Literature Review

Some of the older works addressed the problem of segmenting the region of intracerebral hemorrhages.[1] Earlier work by researchers used a spatially weighted k-means histogram-based clustering algorithm. Some authors applied a multi-resolution simulated annealing method. A more modern work a thresholding technique based on FCM clustering to remove all non-brain regions.[2] The results use median filtering to eliminate noise in the image, and then the maximum entropy threshold was computed for each slice to determine the potential abnormal regions as hemorrhage. Region growing is not often used alone because it is not sufficient to segment brain structures accurately and robustly.

Generalized fuzzy c-means algorithm uses both pixel attributes and local spatial information that is weighted in correspondence with neighbor elements based on their distance attributes.[3] A result of the unsupervised segmentation seems to be highly stable, but a comparison with standard unsupervised methods (k-means) is not very significant in the clinical environment as a consequence of the segmentation of multivariate medical images. A symmetric based result constitutes the initialization of a segmentation method based on a combination of a deformable model and spatial relations, leading to a precise segmentation of the abnormalities.[4] An enhancement process is applied to improving the quality of images along with mathematical morphology to increase the contrast in MRI images. Wavelet can assist in detecting hemorrhage through large sets of MRI of brain scans within a very small time period.[5]

Proposed Methodology

The data set of image database[6,7] of T1, T2, and PD MR image containing multiple image slices has been used here. The RGB image has been converted to a grayscale image using a weighted sum of the R, G, and B components multiplied by a constant. The transformation function is given below,

$$g(x,y) = T[f(x,y)] \quad (1)$$

Here f(x, y) is the input image, g(x, y) is the processed image, and T is an operator on f, defined over some neighborhood of f(x, y). Also, T can operate on a set of input images. The simplest form of T is when the neighborhood is of size 1×1 (that is, a single pixel). In this case, g depends only on the value of f at (x, y), and T becomes a gray-level (also called an intensity or mapping) transformation function of the form as shown below:

$$s = T(r) \quad (2)$$

For maintaining simplicity in notation, r and s are variables denoting, respectively, the gray level of f(x, y) and g(x, y) at any point (x, y). This conversion is followed by image binarization, constituting the preprocessing step and threshold intensity is calculated by the standard deviation of the image pixel intensity. To calculate the standard deviation, mean and variance derivation is written below. Mean is defined as the division of the number of samples multiplied by the sum of all data points as shown in equation 3.

$$\mu = \frac{1}{MN}\sum_{x=0}^{M-1}\sum_{y=0}^{N-1} f(x,y) \quad (3)$$

Variance, is denoted as v, equals one divided by the number of samples minus one, multiplied by the sum of each data point subtracted by the mean then squared. This is given in equation 4.

$$v = \frac{1}{MN}\sum_{x=0}^{M-1}\sum_{y=0}^{N-1} (f(x,y) - \mu)^2 \quad (4)$$

Standard deviation, denoted as σ, equals the square root of the variance s-squared is written below,

$$\sigma = \sqrt{v} \quad (5)$$

The obtained standard deviation intensity value is used as threshold intensity to binarize the MR image of the brain and is very much helpful for extracting brain portion and differentiating it from to the non-brain portion. MRI of the brain has the significant intensity difference between the background and the foreground, so the use of standard deviation based binarization has been successfully implemented for brain stroke detection purpose.

$$f1(x,y) = \begin{cases} 1 & \text{if } f(x,y) > \sigma \\ 0 & \text{if } f(x,y) \le \sigma \end{cases} \quad (6)$$

The negative of an image with gray levels in the range [0, L-1] is obtained by using the negative transformation is given by the expression,

$$s = L - 1 - r \quad (7)$$

Reversing the intensity levels of an image in this manner produces the equivalent of a photographic negative, and this type of processing is particularly suited for enhancing white or gray detail fixed in dark regions of an image, especially when the black areas are dominant in size. For binary image complement, the algorithm use f2(x,y)=1-f1(x,y) which prepare it for the next step of wavelet decomposition. We begin by defining the wavelet series expansion of function f2(x) ϵ $L^2(R)$ relative to wavelet ψ(x) and scaling function φ(x). f2(x) can be represented by a scaling function expansion and some number of wavelet function expansions in sub-spaces Wj0, Wj0+1, Wj0+2 ….. Thus

$$f2(x) = \sum_k c_{j_0}(k)\varphi_{j_0}(x) + \sum_{j=j_0}^{\infty}\sum_k d_j(k)\psi_{j,k}(x) \quad (8)$$

Here j0 is an arbitrary starting scale and the cj0(k), and dj(k) are relabeled. The cj0(k) normally called approximation or/and scaling coefficients; the dj(k) are referred to as detail or/and wavelet coefficients. Thus in the above equation first sum uses scaling function to provides an approximation of f2(x) at scale j0. For each higher scale j ≥ j0 in the second sum, a finer resolution function a sum of the wavelet is added to the approximation to provide increasing details. If the expansion function forms an orthogonal basis or tight frame, which is often the case, the expansion coefficients are calculated and is shown in the equations below,

$$c_{j_0}(k) = \langle f2(x), \varphi_{j_0}(x)\rangle = \int f2(x)\,\varphi_{j_0}(x)\,dx$$

and

$$d_j(k) = \langle f2(x), \psi_{j,k}(x)\rangle = \int f2(x)\,\psi_{j,k}(x)\,dx \quad (9)$$

Above two coefficients expansion are defined as inner products of a function being expanded and the expansion functions being used where φ_{j_0} and $\psi_{j,k}$ are the expansion functions; c_{j_0} and d_j are the expansion coefficients. Two-dimensional (2-D) scaling function, φ(x,y), which is a product of two 1-D functions and three two-dimensional wavelets, $\psi^H(x,y)$, $\psi^V(x,y)$ and $\psi^D(x,y)$ are required. Excluding the products that produce 1-D results, like φ(x) ψ(x), the four remaining products create the separable scaling function and separable directionally sensitive wavelets,

$$\varphi(x,y) = \varphi(x)\varphi(y) \quad (10)$$

$$\psi^H(x,y) = \psi(x)\psi(y) \quad \psi^V(x,y) = \psi(x)\psi(y)$$

$$\psi\text{^}D\ (x,y) = \psi(x)\psi(y) \quad (11)$$

The wavelets measure functional variations, intensity variations for images along different directions: ψ^H measures variations along columns, ψ^V measures variations along rows and ψ^D measures variations along diagonals.

The directional sensitivity is a natural consequence of separability in the above equation 11 and it does not increase the computational complexity. The method first defines the scaled and translated basis functions:

$$\varphi_{j,m,n}(x,y) = 2^{\frac{j}{2}}\varphi(2^j x - m, 2^j y - n)$$
$$\psi^i{}_{j,m,n}(x,y) = 2^{\frac{j}{2}}\psi^i(2^j x - m, 2^j y - n), \quad i = \{H,V,D\} \qquad (12)$$

Here index i identifies the directional wavelets. The discrete wavelet transforms of image f2(x, y) of size M×N is then denoted by the following equations,

$$W_\varphi(j_0,m,n) = \frac{1}{\sqrt{MN}}\sum_{x=0}^{M-1}\sum_{y=0}^{N-1} f2(x,y)\varphi_{j_0,m,n}(x,y)$$
$$W_{\psi^i}(j,m,n) = \frac{1}{\sqrt{MN}}\sum_{x=0}^{M-1}\sum_{y=0}^{N-1} f2(x,y)\psi^i{}_{j,m,n}(x,y), \quad i = \{H,V,D\} \qquad (13)$$

As in the 1-D case, j_0 is an arbitrary starting scale and the $W_\varphi(j_0,m,n)$ coefficients define an approximation f2(x, y) at scale j_0. The $W_{\psi^i}(j,m,n)$ coefficients add horizontal, vertical, and diagonal details for scales $j \geq j_0$. normally $j_0=0$ and $N=M=2^j$ so that $j=0,1,2,\ldots,J-1$ and $m=n=0,1,2,\ldots,2^j-1$. Thus f2(x, y) is obtained via the inverse discrete transform as obtained by the equation,

$$f2(x,y) = \frac{1}{\sqrt{MN}}\sum_m\sum_n W_\varphi(j_0,m,n)\varphi_{j_0,m,n}(x,y) + \frac{1}{\sqrt{MN}}\sum_{i=H,V,D}\sum_{j=j_0}^{\infty}\sum_m\sum_n W_{\psi^i}(j,m,n)\psi^i{}_{j,m,n}(x,y) \qquad (14)$$

After applying wavelet decomposition up to level, two non-brain regions are totally separated from the brain in a discrete form which is not useful for the approach as there is a possibility that abnormality may get lost and to rectify this problem a quick hull algorithms as proposed in[8] is implemented. The convex hull of a set of points in the plane is the shape taken by a rubber band that is placed "on the points" and allowed to shrink to a state of equilibrium. A point can represent in the plane by a pair (x,y) that stores the x and y Cartesian coordinates for that point. A line l as a triple (a,b,c), such that these values are the coefficients a, b, and c of the linear equation ax+by+c = 0 associated with l. Given the Cartesian coordinates (x1, y1) of q1 and (x2, y2) of q2, the equation of the line l through q1 and q2 is given by,

$$\frac{x - x_1}{x_2 - x_1} = \frac{y - y_1}{y_2 - y_1} \qquad (15)$$

Constants a, b, and c can be derived as $a = (y_2-y_1)$; $b = -(x_2-x_1)$; and $c = y_1(x_2- x_1) - x_1(y_2 -y_1)$. A line segment s1 is typically represented by the pair (p,q) of points in the plane that form s1's end points. It is possible to represent a polygon P by a circular sequence of points, called the vertices of P. The segments between consecutive vertices of P are called the edges of P. Polygon P is said to be nonintersecting, or simply if intersections between pairs of edges of P happen only at a common endpoint vertex.

A polygon is convex if it is simple and all its internal angles are less than p. Quick-hull described in[8] is a divide-and-conquer algorithm, similar to quicksort, which divides the problem into two sub-problems and discards some of the points in the given set as interior points, concentrating on remaining points. Quick-hull runs faster than the randomized algorithms because it processes fewer interior points. Also, Quick-hull reuses the memory occupied by old facets. The convex image is now a binary image in which only brain portion is denoted with one, and all non-brain portion contains zero. This convex image is multiplied with the original image and the resultant image is free of any previously existing artifacts, noise and skull as such removals are critical for brain abnormality detection.

RESULTS AND DISCUSSION

Proposed methodology has been applied to the hemorrhage and the results on that abnormalities have been describing in this section.

In Figure 1 hemorrhage has been found on the left lobe of the brain. There is no relation with the skull portion, and it is classified as cerebral and intracranial hemorrhage. In the experiments conducted, the algorithm is implemented on T2, T1 and PD type of MRI images for cerebral hemorrhage detection and the methods successfully detected an abnormality, but when applying to other kinds of hemorrhage detection, the skull elimination steps are excluded (in preprocessing skull removal is optional). The images shown in Figure 1 belong to a 49-year-old African-American woman[6] with a history of hypertension and diabetes mellitus. The scan was performed when the patient experienced numbness and tingling of the left leg for about one day. Systemic arterial blood pressure was 240/130. There was no weakness, facial droop, visual change; no upper extremity or right lower extremity sensory abnormality; no bowel or bladder dysfunction; no headache, fever, shortness of breath, chest pain, nausea, vomiting, diaphoresis, vertigo or light-headedness, no back pain, and no history of seizures.

An epidural hematoma is located into the potential space between the dura, which is inseparable from cranial periosteum and the adjacent bone. A Subdural hematoma is diagnosed by mass effect, which is depicted as the

displacement of the blood vessels on angiograms on the skull. Subarachnoid hemorrhage appears when bleeding happens into the subarachnoid space around the brain and spinal cord. The testing dataset[6] consists of 460 MRI images of the human brain with a different type of hemorrhage including some normal brain image. Among the images, 40 are of the normal brain while the remaining images represent brains with at least one of the three types of the brain hemorrhage. An image of a normal brain shows a distribution of gray matter that appears clear in the texture-like fissures, while an abnormal brain has a shape which appears brighter than the normal gray matter. Abnormal regions of the brain differ in characteristics than the normal brain, but the diversity of characteristics is notable when compared to any other organ for T1, T2 and PD type of MRI images. Thus accurate segmentation is very important and considerable attention has been given to achieve the same. For brain hemorrhage segmentation several steps have been proposed and details are shown in Figure 1 below. Figure 1(a) is the input MRI of the brain and Figure 1(b) is after applying artifacts and skull removal method. Figure 1(c) is the output image after power law transformation has been applied on the convexed image which is helpful to segment the brain hemorrhages. Figure 1 (d) shows binary segmented hemorrhage portion. In Figure 1(e) depicts the hemorrhage portion within the brain image marked by red region for visualization. Figure 1(f) shows the contour detection by horizontal contour detection and Figure 1(g) show the vertical contour detection. Contour lines are not continuous for the horizontal and vertical contour that is why both are combined to obtain the final contour image which is continuous and is shown in Figure 1(h). Figure 1(i) shows the localization of hemorrhage and accordingly classified based on their localization information into different types of the brain hemorrhage.

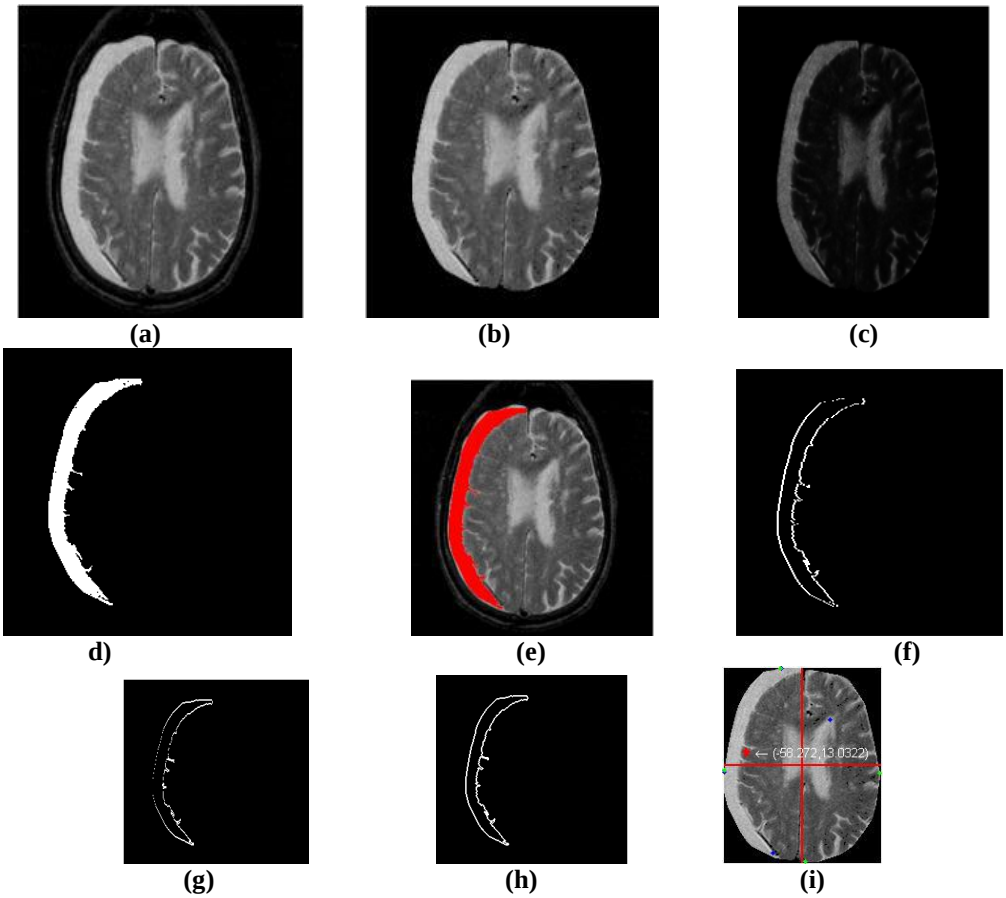

Figure 1: Hemorrhage segmentation results. a) Input MRI of the brain, b) applying artifacts and skull removal, c) after gamma transformation, d) segmented abnormal portion, e) abnormal portion indicated by red marks, f) horizontal contour, g) vertical contour, h) contour of abnormal region, i) localization of abnormal region.

It is very clear from chronic subdural hematoma segmentation that it has an elliptic nature and area large respect to other. The position of segmented lesion differs from another type of hemorrhage. Intraparenchymal hemorrhage generally smaller in size and its position not nearer to skull.

CONCLUSIONS

Accurate measurements of abnormalities in Hemorrhage from MRI scan have been successfully implemented by the proposed system. This is critical for early, reliable and accurate detection of tumor, stroke and hematoma for providing early diagnosis and treatment, prompt transfer of the patient to a medical facility capable of

MRI scanning and neurological intervention if necessary. Automated systems for analyzing and classifying medical images have gained a great level of attention and the methods proposed will positively contribute to the betterment of such system.

REFERENCES

1. S. Loncaric and Z. Majcenic, "Multiresolution simulated annealing for brain image analysis: In Medical Imaging," International Society for Optics and Photonics, 1999; 1139–1146.
2. Y. Li, Q. Hu, J. Wu, and Z. Chen, "A hybrid approach to detection of brain hemorrhage candidates from clinical head ct scans," In Sixth International Conference on Fuzzy Systems and Knowledge Discovery (FSKD), pages 361–365, 2009 [114] Van Lung, J. M, Kim, "A generalized spatial fuzzy c-means algorithm for medical image segmentation," IEEE International Conference on Fuzzy systems, IEEE, 2009; 409-414.
3. Van Lung, J. M, Kim, "A generalized spatial fuzzy c-means algorithm for medical image segmentation," IEEE International Conference on Fuzzy systems, IEEE, pp. 409-414, 2009.
4. Hassan Khotanlou, Olivier Colliot and Isabelle Bloch, "Automatic brain tumor segmentation using symmetry analysis and deformable models," Ecole Nationale Superieure des Telecommunications, 2015; 1-6.
5. A. Kharrat, N. Benamrane, M. Ben Messaoud, M Abid, "Detection of brain tumor in medical images," 3rd International Conference on In Signals, Circuits and Systems (SCS), Proc. IEEE, 2012; 1-6.
6. Whole Brain Atlas: MR brain image [online (2013): http://www.med.harvad.edu/AANLIB/home.html].
7. The EASI MRI Home: MR brain image [online (2013): http://www.easidemographics.com/cgi-bin/dbmri.asp].
8. C. Bradford Barber, David P. Dobkin, Hannu Huhdanpaa, "The Quickhull Algorithm for Convex Hulls", ACM Transactions on Mathematical Software, 1996; 22(4): 469–483.